



Contents lists available at ScienceDirect

Journal of Immunological Methods

journal homepage: [www.elsevier.com/locate/jim](http://www.elsevier.com/locate/jim)

## Probability state modeling of memory CD8<sup>+</sup> T-cell differentiation<sup>☆</sup>

Margaret S. Inokuma<sup>a,\*</sup>, Vernon C. Maino<sup>a</sup>, C. Bruce Bagwell<sup>b</sup>

<sup>a</sup> BD Biosciences, 2350 Qume Drive, San Jose, CA 95131, USA

<sup>b</sup> Verity Software House, P.O. Box 247, Topsham, ME 04086-0247, USA

### ARTICLE INFO

#### Article history:

Received 22 April 2013

Received in revised form 29 July 2013

Accepted 4 August 2013

Available online xxxxx

#### Keywords:

Probability state modeling

Flow cytometry

Immunomics

CD8 T cells

Computational model

Data analysis

### ABSTRACT

Flow cytometric analysis enables the simultaneous single-cell interrogation of multiple biomarkers for phenotypic and functional identification of heterogeneous populations. Analysis of polychromatic data has become increasingly complex with more measured parameters. Furthermore, manual gating of multiple populations using standard analysis techniques can lead to errors in data interpretation and difficulties in the standardization of analyses. To characterize high-dimensional cytometric data, we demonstrate the use of probability state modeling (PSM) to visualize the differentiation of effector/memory CD8<sup>+</sup> T cells. With this model, four major CD8<sup>+</sup> T-cell subsets can be easily identified using the combination of three markers, CD45RA, CCR7 (CD197), and CD28, with the selection markers CD3, CD4, CD8, and side scatter (SSC). PSM enables the translation of complex multicolor flow cytometric data to pathway-specific cell subtypes, the capability of developing averaged models of healthy donor populations, and the analysis of phenotypic heterogeneity. In this report, we also illustrate the heterogeneity in memory T-cell subpopulations as branched differentiation markers that include CD127, CD62L, CD27, and CD57.

© 2013 The Authors. Published by Elsevier B.V. All rights reserved.

### 1. Introduction

In recent years, much effort has been applied to understanding the differentiation pathways from naïve CD8<sup>+</sup> T cells to memory and effector subsets (Appay et al., 2008; Arens and Schoenberger, 2010; Obar and Lefrancois, 2010). Early descriptions of CD8<sup>+</sup> T-cell differentiation states identify populations based on surface and functional markers expressed by T cells in response to various antigens. As an example, naïve T cells have high-proliferative capacity but do not express effector cytokines such as IFN- $\gamma$  (Geginat et al., 2003). Although cell surface

marker phenotypes and functions have been assigned to subsets within this differentiation pathway, a precise discrimination of effector and memory CD8<sup>+</sup> T cells has proven to be complex and controversial due to the heterogeneity of the subsets (Bachmann et al., 2005; Hamann et al., 1997; Stemmerger et al., 2009; Tomiyama et al., 2002). These definitions are further complicated by lack of consensus for phenotypic markers that define CD8<sup>+</sup> T-cell subsets. Sallusto et al. (1999) first defined T-cell memory subsets with CD45RA, CCR7, and CD62L. Others have identified long-term memory subsets with CD127 and CD62L (Kaech et al., 2003). A recent study by Appay et al. has defined five distinct CD8<sup>+</sup> T-cell subsets based on correlated single-cell measurements (Appay et al., 2008).

Rapid advances in flow cytometry have resulted in the ability to resolve up to 17 biomarkers associated with a single cell (Chattopadhyay et al., 2006). This capability has enabled the description of new cellular subsets and consequent differentiation pathways. However, analysis of high-dimensional data has proven challenging. Traditional methods often involve the gating of populations in one- or

*Abbreviations:* CDP, control definition point; CM, central memory; EF, terminal effector; EM, effector memory; EP, expression profile; PBMCs, peripheral blood mononuclear cells; PCA, principal components analysis; PSM, probability state modeling; SPLOM, scatterplot matrix; SSC, side scatter.

<sup>☆</sup> This is an open-access article distributed under the terms of the Creative Commons Attribution License, which permits unrestricted use, distribution, and reproduction in any medium, provided the original author and source are credited.

\* Corresponding author.

E-mail addresses: [Margaret\\_Inokuma@bd.com](mailto:Margaret_Inokuma@bd.com) (M.S. Inokuma), [Vernon\\_Maino@bd.com](mailto:Vernon_Maino@bd.com) (V.C. Maino), [cbb@vsh.com](mailto:cbb@vsh.com) (C.B. Bagwell).

0022-1759/\$ – see front matter © 2013 The Authors. Published by Elsevier B.V. All rights reserved.

<http://dx.doi.org/10.1016/j.jim.2013.08.003>

Please cite this article as: Inokuma, M.S., et al., Probability state modeling of memory CD8<sup>+</sup> T-cell differentiation, J. Immunol. Methods (2013), <http://dx.doi.org/10.1016/j.jim.2013.08.003>

two-dimensional displays and manually selecting populations of interest. Such methods are highly subjective, time consuming, not easily scalable to a high number of dimensions, and inherently inaccurate because they do not account for population overlap. Automated gating algorithms can reduce the subjectivity of manual gating and thereby improve reproducibility but are generally limited to two-dimensional projections of the data and do not account for overlapping populations. Neither of these methods addresses the issue of visualizing the biology of complicated cellular progressions defined by many correlated measurements in a simple, objective format. The development of novel bioinformatics tools is needed to interpret expression changes in a wide variety of proteins for a number of cell subtypes.

Many groups have addressed these challenges with a variety of approaches for data analysis (Aghaeepour et al., 2012; Bashashati and Brinkman, 2009; Lugli et al., 2010). A number of these approaches involve some variation of clustering analysis, which can have considerable limitations. For example, an important option in clustering is setting the desired number of clusters and the cluster linkage thresholds. If the selection of these setup options is not determined automatically, then different operators are likely to get different answers, resulting in lack of reproducibility. In addition, many clustering analysis approaches are not optimized to identify marker expression transitions between clusters. These transitions are characteristic of the biological systems they represent and therefore are equally as important, if not more biologically relevant, than recognizing distinct clusters. Another issue that has limited the practicality of clustering is that many of the algorithms are not scalable to any number of dimensions and events. An often overlooked limitation of these methods is that many require the user to evaluate the identified clusters with numerous two-dimensional dot plots, complicating the effective scalability of the method with an increased number of correlated measurements.

Other approaches have been developed in addition to clustering, including principal components analysis (PCA) (Costa et al., 2010) and Bayesian inference (Sachs et al., 2009). These and similar approaches (Zare et al., 2010) have been evaluated through the FlowCAP initiative (<http://flowcap.flowsite.org/>). One unique approach, an algorithm called SPADE, utilizes down-sampling, clustering, minimum spanning tree, and up-sampling algorithms to generate two-dimensional branched visualizations (Qiu et al., 2011). The branched-tree structure incorporates information from all measurements in the data, partially addressing scalability issues. However, SPADE has many of the same subjective inputs as conventional clustering algorithms (e.g., number of clusters) and also may have issues of reproducibility and generation of non-biological branches.

In this study, we demonstrate the utility of *probability state modeling* (PSM) (Bagwell, 2011, 2012, 2010, 2007) and the visualization tools in GemStone™ software in the analysis of multidimensional flow cytometry data. A probability state model is a set of generalized Q functions, one for each correlated measurement, where the common cumulative probability axis can be a surrogate for time or cellular progression. By exploiting the unique characteristics of Q functions, PSM can model any number of correlated measurements and present one comprehensive yet understandable view of the results. PSM is fully

described in the Supplementary Materials Section of this paper. This model uses an unbiased approach for identification of cell subpopulations, eliminating the subjectivity introduced with manual gating.

Using this approach, we constructed a probability state model for CD8<sup>+</sup> T-cell antigen-dependent progression that can automatically analyze cytometric list-mode data derived from T-cell-specific panels of antibodies. We describe the design of the model, demonstrate its reproducibility, and also show how a group of normal donor samples can be represented by a single probability state model, resulting in an automated visualization of multidimensional data. In the seminal review article by Appay et al. (2008), a graphical representation of CD8<sup>+</sup> T-cell pathway differentiation was deduced from multiple files of manually gated data. PSM enables the correlated visualization of multiple phenotypic biomarkers, allowing for the characterization of T-cell differentiation. Using the technology presented in this study, T-cell subsets and differentiation can be phenotypically characterized for each patient sample. By evaluating Pearson correlations between the model parameters, we show that there are only four CD8<sup>+</sup> T-cell stages defined by CD3, CD8, CD4, CCR7 (CD197), CD28, and CD45RA, not five as has been previously reported (Appay et al., 2008). We also show using PSM in this analysis that some traditional T-cell markers such as CD62L, CD27, CD57, and CD127 can delineate branched pathways of CD8 T-cell differentiation.

## 2. Materials and Methods

### 2.1. Flow cytometry acquisition of human peripheral blood

Peripheral blood was collected after obtaining informed consent from 36 healthy volunteers ranging in age from 30 to 65 years, with a median age of 47.5 years.

**Table 1**  
Monoclonal antibodies.

Antigen	Clone	Fluorophore	Cat. No.	Isotype
CD3	SP34-2	BD Horizon V450	560351	Ms IgG <sub>1</sub>
CD3	SK7	APC-H7	641397	Ms IgG <sub>1</sub>
CD3	SK7	FITC	340542	Ms IgG <sub>1</sub>
CD4	RPA-T4	BD Horizon™ V500	560768	Ms IgG <sub>1</sub>
CD4	SK3	PerCP-Cy™ 5.5	341654	Ms IgG <sub>1</sub>
CD4	RPA-T4	BV605	562658	Ms IgG <sub>1</sub>
CD8	SK1	APC-H7	641409	Ms IgG <sub>1</sub>
CD8	RPA-T8	BD Horizon™ V500	560775	Ms IgG <sub>1</sub>
CD8	SK1	PerCP-Cy™ 5.5	341051	Ms IgG <sub>1</sub>
CD27	L128	APC	655019	Ms IgG <sub>1</sub>
CD27	M-T271	Alexa Fluor® 700	560611	Ms IgG <sub>1</sub>
CD28	L293	PerCP-Cy™ 5.5	337181	Ms IgG <sub>1</sub>
CD28	CD28.2	APC	559770	Ms IgG <sub>1</sub>
CD45RA	L48	PE-Cy7™	337167	Ms IgG <sub>1</sub>
CD56	B159	Alexa Fluor® 700	561902	Ms IgG <sub>1</sub>
CD56	NCAM16.2	BV421	562751	Ms IgG <sub>2b</sub>
CD57	HNK-1	FITC	340706	Ms IgM
CD62L	SK11	FITC	347443	Ms IgG <sub>2a</sub>
CD62L	DREG-56	BD Horizon™ V450	560440	Ms IgG <sub>1</sub>
CD127	HIL-7R-M21	PE	557938	Ms IgG <sub>1</sub>
CCR7	150503	PE	560765	Ms IgG <sub>2a</sub>
CCR7	150503	PE-CF594	562381	Ms IgG <sub>2a</sub>
CCR7	150503	PerCP-Cy™ 5.5	561144	Ms IgG <sub>2a</sub>

Blood samples were collected into BD Vacutainer® CPT tubes (BD Preanalytical Systems) and processed according to product directions. Peripheral blood mononuclear cells (PBMCs) were washed in Stain Buffer (BSA, BD Biosciences, CA). Cells were then incubated for 30 min in Stain Buffer with the manufacturer's suggested dilutions of fluorescently labeled primary monoclonal antibodies (Table 1). The supernatant was aspirated, BD FACSTM lysing solution (BD Biosciences) was added, and each tube was mixed and incubated for 10 min at room temperature. Cells were washed and the supernatant aspirated. All data from samples was acquired using a special order BD™ LSR II flow cytometer and BD FACSDiva™ software (BD Biosciences, CA).

## 2.2. Probability state modeling (PSM)

PSM is a technique that allows high-dimensional modeling and display of data produced by image and flow cytometers. GemStone™ version 1.0.69 (Verity Software House, Topsham, Maine, USA) was used for all PSM analyses. The Supplementary Materials Section describes the theory behind this new approach to data analysis.

## 3. Results

### 3.1. Probability state modeling (PSM)

In cytometry, correlated cellular markers are measured on a per-cell basis. Typically, the correlations between the markers are measured using dot plots. PSM enables flow cytometry data to be visualized using a novel approach. The use of parametric plots allows for the visualization of transitional events and results in the ability to correlate multiple markers. To illustrate the basic principles, a description of how PSM summarizes the timing of two marker expression transitions is shown in Fig. 1. This figure also describes how the model can be used to stage a cellular progression in a mathematically rigorous manner. The theoretical underpinnings of PSM are discussed more fully in the Supplementary Materials Section.

Fig. 1A shows a dot plot where each gray dot represents 1 of 50,000 synthesized events for two correlated measurements, features A and B. There are three observable clusters of events: C1 (gray ellipse), C2 (red ellipse), and C3 (blue ellipse), with transitional events between them. If it is known that features A and B are part of a progression, and A has a low level of

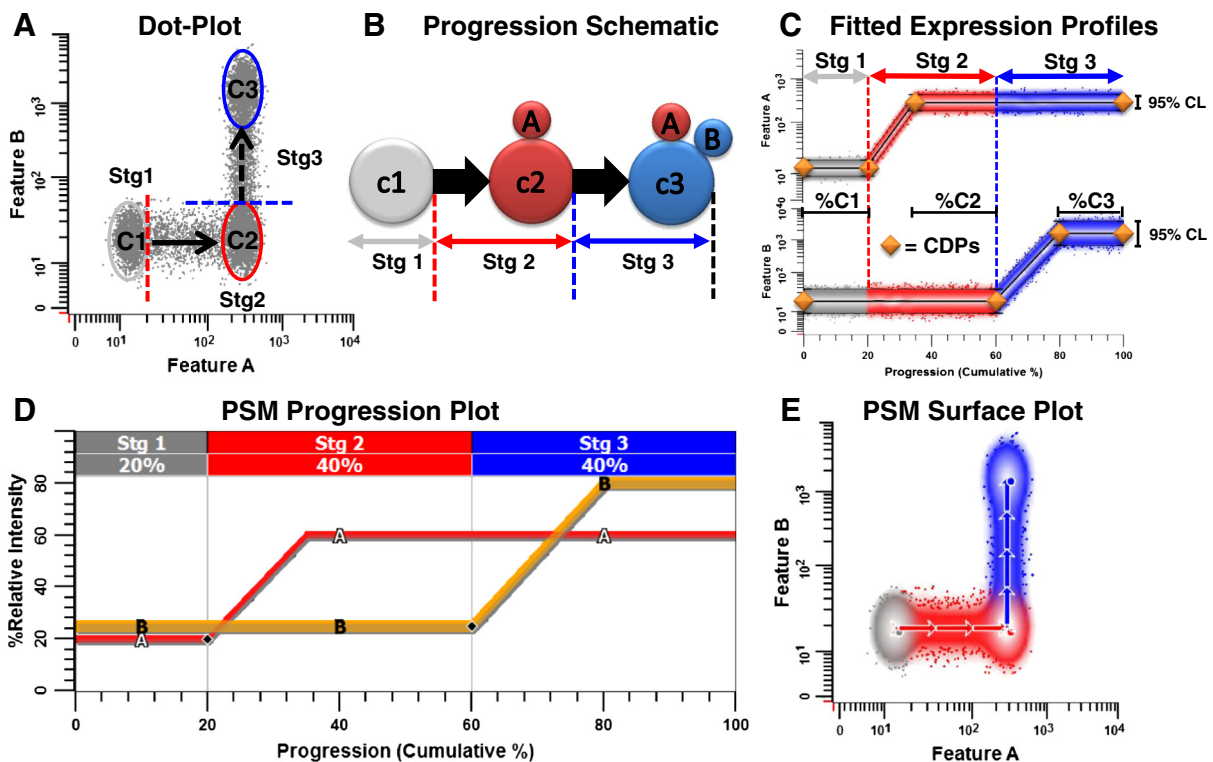


**Fig. 1.** PSM and staging. Panel A shows a dot plot where each gray dot represents a synthesized event expressing two correlated measurements, features A and B. There are three clusters: C1 (gray ellipse), C2 (red ellipse), and C3 (blue ellipse), with transitional events between them. If it is known that features A and B are part of a progression and A has low intensity early and high late (see solid black arrow), then it can be inferred that 1) feature B is also low early and high late, and 2) B is likely to be up-regulated after A (see black dashed arrow). Features A and B can be used to form a staging system for the progression (see dotted red and blue lines for stage boundaries). Panel B shows a schematic of this progression from a single cell's perspective. Given this general information about the progression, a probability state model can be created. Panel C shows the model's EPs for features A and B as defined by their fitted CDPs (orange diamonds). Since the data for each feature is modeled as a relatively small number of CDPs for each measurement, and the x-axis is represented as cumulative percentage, an overlay can be created that summarizes all correlations and percentages in a progression (see Panel D). A probability state model can be projected onto any bivariate as a surface plot, where stage colors are appropriately blended and the projection direction is shown with arrows (see Panel E).

intensity early and high late (see the solid black arrow), then it can be inferred that (1) feature B is also low early and high late and (2) B is likely to be up-regulated after A (see the black dashed arrow). Thus, features A and B can be used to form a logical staging system for the progression. Stage 1 can be defined as those cells that do not express either feature A or B, Stage 2 is those cells that begin to express feature A but have not yet up-regulated feature B, and Stage 3 is those cells that express feature A and begin to show low levels of feature B (see dotted red and blue lines for stage boundaries).

Fig. 1B shows this staging from the point of view of a single cell. A C1 type of cell becomes a c2 when it begins to express feature A, and the c2 cell becomes a c3 when it begins to express feature B. Cytometrists have used this type of logical inference about the timing of multiple markers, when given some initial directionality information, to better understand complex cellular progressions (Loken and Wells, 2000).

Utilizing this general information about the progression, a probability state model can be created and fitted in a manner that is consistent with the observed data. Fig. 1C shows the modeled expression profiles (EPs) for features A and B as defined by their fitted control definition points (CDPs, orange diamonds). In PSM, the density of events is constant along the *x*-axis, transforming this axis to cumulative percentage (see the *x*-axis). The percent of events that are in clusters C1 (20%), C2 (25%), and C3 (20%), as well as Stages 1 (20%), 2 (40%), and 3 (40%), can be read directly from the *x*-axis. PSM accounts for population overlap and requires no gating (for details, see the Supplementary Materials Section). It also enables the visualization of measurement variability with 95% confidence limits (CLs, see Fig. 1C), which are a function of measurement uncertainty and biologic heterogeneity. The relative widths of the expression profiles for features A and B show that the CLs of B are twice that of A. Since PSM reduces complex high-dimensional data into a relatively small number of CDPs for each measurement, an overlay or “progression plot” can be created that summarizes all correlations and percentages in a progression (see Fig. 1D). The thicknesses of the bands in the progression plot are proportional to the 95% CLs. A probability state model can be projected onto any bivariate as a surface plot, where stage colors are appropriately blended and the projection direction is shown with arrows (see Fig. 1E).

### 3.2. Addressing the dimensionality barrier

A single PSM progression plot can represent thousands of dot plots with very high-dimensional data (Inokuma et al., 2010), while unambiguously showing biological changes that accompany complex cellular progressions. Fig. 2 demonstrates this important characteristic of PSM using one of this study's CD8<sup>+</sup> T-cell samples. Fig. 2A shows the probability state model progression plot derived from a list-mode file containing the correlated measurements of CD3, SSC, CD8, CD4, CCR7 (CD197), CD28, and CD45RA. The *x*-axis represents CD8<sup>+</sup> T-cell memory and effector differentiation with units of cumulative percent of events. The *y*-axis is the relative dynamic range of the measurement intensities between 0 and 100. The end of the naïve stage (red) is defined as the beginning of the down-regulation of CD45RA (see the first black diamond). The end of the central memory (CM, green)

stage is defined by the down-regulation of CD28 (see the black diamond), and the end of the effector memory stage (EM, blue) and the beginning of the terminal effector cell stage (EF, brown) are at the point where CD45RA ceases to up-regulate (see the second black diamond). Each CDP defines the shape of the expression profile. In an EP, the CDP is shown as a white or black diamond.

Fig. 2B shows scatterplot matrix (SPLOM) plots of all combinations of CD3, SSC, CD8, CD4, CCR7 (CD197), CD28, and CD45RA (7 single and 21 two-parameter dot plots). The plot surfaces are appropriately blended with the stage colors, and the dots shown are events in the tails of the 95% confidence limits of the probability state model EPs. All the information represented in the 28 plots in Fig. 2B is shown in the one progression plot in Fig. 2A, demonstrating how PSM circumvents the dimensionality barrier that accompanies typical cytometric analysis systems.

### 3.3. Model averaging and reproducibility

Since PSM effectively reduces a list-mode file into a relatively small set of model parameters known as CDPs, it is possible to model a set of files and obtain statistics such as means, standard deviations (SDs), and Pearson correlations for all the CDPs modeled. These statistically determined CDPs can then be used to construct a progression plot that represents an average of all the files in a group. The variabilities from this averaged model can be represented as box whiskers (– range, – 95% CL, mean, + 95% CL, + range). The first use of this averaging capability was to evaluate the reproducibility of the PSM system.

Stained PBMC samples from three healthy donors were acquired in triplicate by the cytometer. All three replicates per donor were modeled and averaged. The results are summarized in Fig. 3A, B, and C. The *x*- and *y*-axes are defined as described in Figs. 1 and 2. Each CDP in the progression plot has a vertical box whisker for examining the variability of measurement intensities and a horizontal box whisker for examining the variability of cumulative percentages. Since the variability of the CDPs are minimal, the data suggest that there is reasonable reproducibility for staining, acquisition, and modeling. Additionally, each donor appears to have unique percentages for each stage, but the phenotypic patterns formed from coordinated marker changes are similar for these three donors, suggesting there is donor to donor variability in the number of cells representing a given stage, but the stages are defined in a biologically prescribed manner.

### 3.4. Average CD8<sup>+</sup> T-cell antigen-dependent progression model

To better understand the coordinated marker changes and CDP variabilities for this progression, an average CD8<sup>+</sup> T-cell model was created from modeling 20 samples of PBMCs from healthy donors with antibodies against CD3, CD4, CD8, CCR7 (CD197), CD28, and CD45RA (see Fig. 4A). The mean and SD (in parentheses) of the stages were %naïve, 25 (13); %CM, 38 (16); %EM, 17 (17); and %EF, 21 (18), shown at the top of the progression plot. The vertical box whiskers show that there is quite a bit of variability in the measurement intensities. This variability is presumably a function of not only donor-to-donor variability, but also instrument setup variability. The horizontal

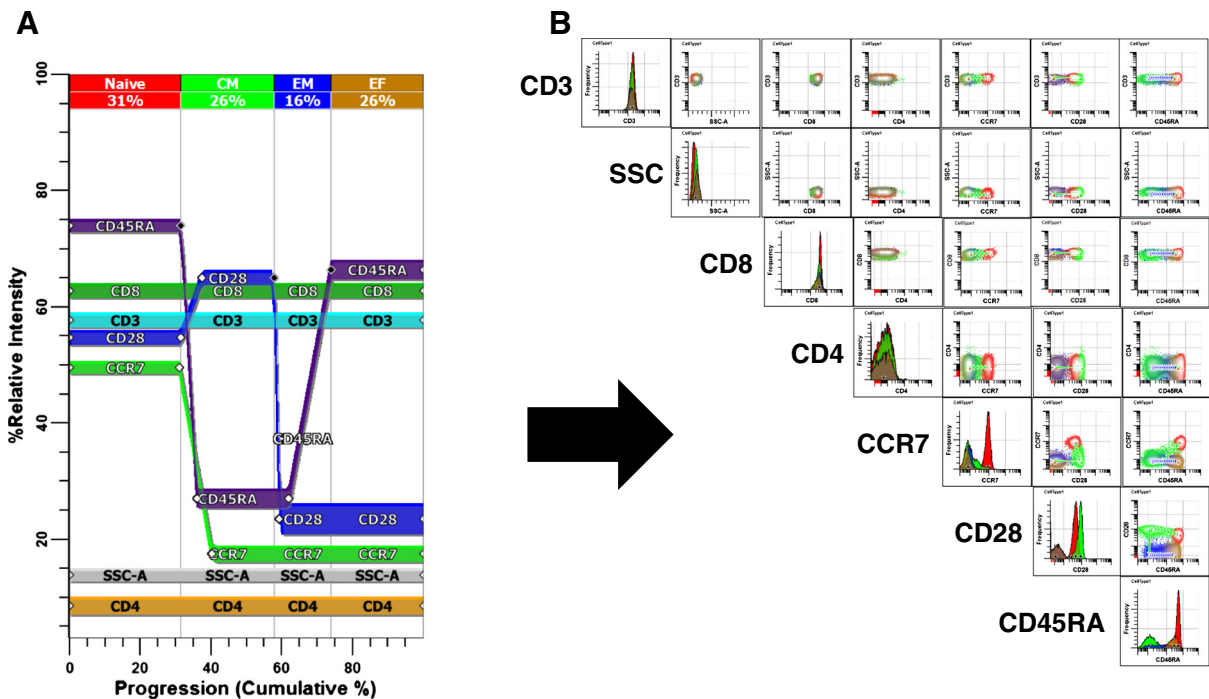


**Fig. 2.** Typical PSM analysis of CD8<sup>+</sup> T cells compared with dot plot surface projections. Panel A shows a probability state model progression plot of CD8<sup>+</sup> T cells defined by the correlated measurements CD3, SSC, CD8, CD4, CCR7 (CD197), CD28, and CD45RA. The x-axis represents CD8<sup>+</sup> T-cell antigen-dependent progression with units of cumulative percentage of events. The y-axis is the relative dynamic range of the measurement intensities between 0 and 100. The end of the naïve stage (red) is defined as the beginning of the down-regulation of CD45RA (see first black diamond). The end of the CM (green) stage is defined by the down-regulation of CD28 (see black diamond), and the end of the EM stage (blue) and the beginning of the EF stage (brown) are the end of the up-regulation of CD45RA (see second black diamond). Each CDP in an EP is shown as a white or black diamond. Panel B shows scatterplot matrix (SPLOM) plots of all combinations of CD3, SSC, CD8, CD4, CCR7 (CD197), CD28, and CD45RA (7 single and 21 two-parameter dot plots). The plot surfaces are appropriately blended with the stage colors, and the dots shown are events in the tails of the 95% CIs of the probability state model EPs. All the information represented in the 28 plots in Panel B is shown in the progression plot in Panel A, demonstrating how PSM circumvents the dimensionality barrier that normally accompanies cytometric analysis systems.

box whiskers show the variations of the CD8<sup>+</sup> subset percentages.

An interesting observation in Fig. 4A is that at the point where T cells down-regulate CD45RA, the expression of CCR7 (CD197) is also down-regulated, suggesting that they may be coordinated to define the end of the naïve stage. Supporting this hypothesis are (1) the statistics of the locations where CD45RA and CCR7 (CD197) down-regulate have a Pearson correlation coefficient, *r*, of 0.85 (*p* < 0.00001), and (2) the difference in locations (CCR7–CD45RA) was –0.51%, which was found to be not significant using a paired *t* test. This correlation data indicate that when CD45RA down-regulates at the end of the naïve stage, CCR7 is indeed down-regulated, while CD28 is minimally up-regulated (see Fig. 4B, blue hatched arrows). Our data are not consistent with the supposition that there is an extra stage as determined by CD45RA<sup>–</sup>CCR7<sup>+</sup>CD28<sup>+</sup> (Appay et al., 2002). Events with this phenotype captured by a gating strategy are most likely a mixture of naïve and CM events as defined by this analysis.

The CD8<sup>+</sup> average model also supports the hypothesis that when CD28 is down-regulated, CD45RA begins to be up-regulated (red arrows, *r* = 0.56, *p* < 0.01 with a difference of 1.9 (NS)). The last EF stage, is defined as the point at which the up-regulation of CD45RA has ended.

### 3.5. Heterogeneity of marker expression (branching)

During the developmental progression of memory and effector T cells, a subset of cells may begin to preferentially express markers that might not be expressed in the remaining cells. In PSM, the heterogeneous expression of markers can be visualized with branching expression profiles (see Fig. 5). Fig. 5A shows a progression schematic similar to Fig. 1 but includes a simple branch involving feature C. In this example, when cells reach the checkpoint where feature B is up-regulated, 70% of the cells also up-regulate feature C, while 30% do not. Fig. 5B delineates the three probability state model EPs that model this simple branch (top = feature A, middle = feature B, and bottom = feature C). Fig. 5C summarizes this progression in the probability state model progression plot, which includes the branching of feature C (see the CB label). Fig. 5D shows the associated probability state model surface dot plots for feature A vs. B (top), feature A vs. C (middle), and feature B vs. C (bottom). Note that branches are not always visible in dot plots, which is why they have been traditionally difficult to detect.

Branches are relatively easy to determine with PSM since non-branched EPs are incompatible with branched data, resulting in a dramatic loss of classified events and poor fitting. In this simple example, the branch point is at the end

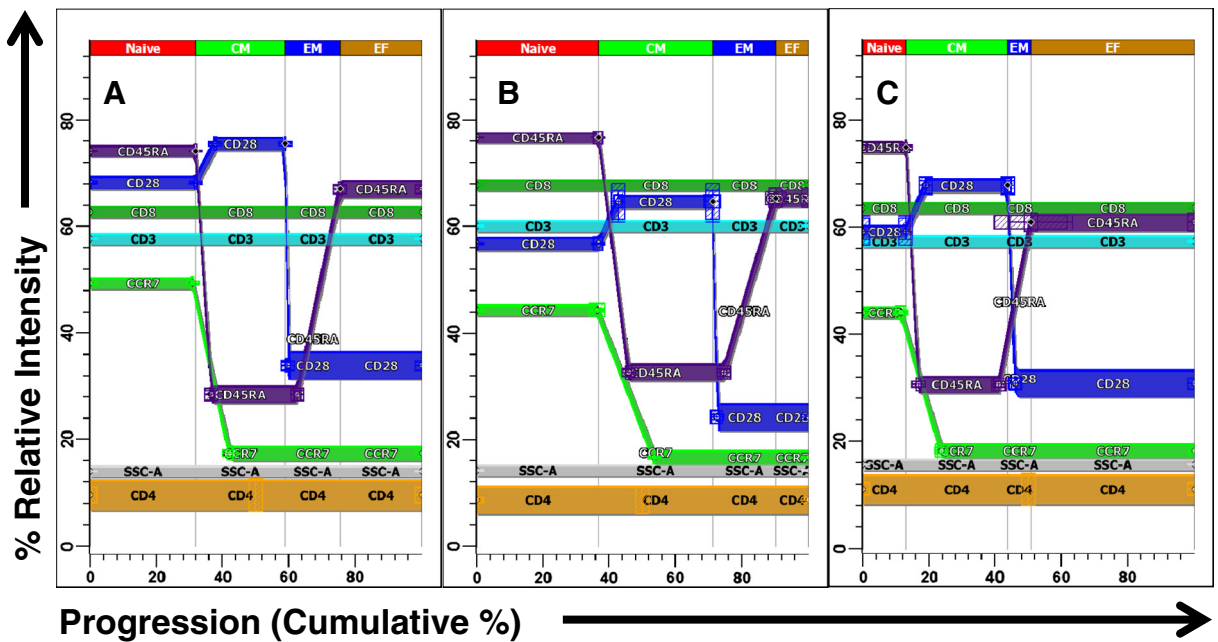


**Fig. 3.** Reproducibility of staining, acquisition, and modeling. Panels A, B, and C are average probability state model progression plots from three replicate samples from three different healthy donors. The  $x$ - and  $y$ -axes are defined as described in Figs. 1 and 2. Each CDP in the progression plot has a vertical box whisker for examining the variability of measurement intensities and a horizontal box whisker for examining the variability of associated cumulative percentages. Since most of the CDP whiskers are very small, the data suggest that there is reasonable reproducibility for staining, acquisition, and modeling. Additionally, each donor appears to have unique percentages for each stage, but the phenotypic patterns formed from coordinated marker changes are similar for these three donors.

of Stage 2. However, when modeling T-cell branches, the location might be elsewhere along the progression axis.

### 3.6. Average CD8<sup>+</sup> T-cell model with branches

An averaged model featuring 22 samples from healthy donors was used to identify branched markers. Each sample was stained with antibodies against CD3, CD4, CD8, CD45RA, CD28, CCR7 (CD197), CD27, CD62L, CD57, and CD127. Fig. 6 shows the stratification expression profiles of CD45RA, CCR7, and CD28 as well as four branched EPs for CD62L, CD27, CD127, and CD57. Here, CD62L (L-selectin) has a 77% (9%) chance of down-regulating slightly before the end of the naïve stage and correlates best with the down-regulation of CCR7 (blue hatched arrows,  $r = 0.81$ ,  $p < 0.00001$ ,  $\text{diff} = -4.23$ , NS). CD27 slightly down-regulates with CD45RA and CCR7 at the end of the naïve stage and then has a 75% (17%) chance of fully down-regulating in the middle of the CM stage.

Interestingly, CD27 correlated best with the beginning of the second expression level for CD45RA (solid red arrows,  $r = 0.90$ ,  $p < 0.00001$ ,  $\text{diff} = 6.00$ ,  $p < 0.0008$ ). CD127 is slightly up-regulated at the end of the naïve stage and then has a 79% (16%) chance of fully down-regulating in the middle of the CM stage. It is highly correlated with the down-regulation of CD28 (solid blue arrows,  $r = 0.86$ ,  $p < 0.00001$ ,  $\text{diff} = -6.79$ ,  $p < 0.02$ ). CD57, an immunosenescence marker, has a 77% (15%) chance of up-regulating at the end of the CM stage. It is also best correlated with the down-regulation of CD28 (solid green arrows,  $r = 0.97$ ,  $p < 0.00001$ ,  $\text{diff} = -3.23$ , NS).

A detailed analysis of the branches (data not shown) indicates that, for the most part, events that were in one

branch were not more likely to be in other branches, suggesting that the mechanisms behind branching are largely independent for these four markers. Fig. 5B summarizes the branch data in terms of a series of probabilistic checkpoints. In the naïve stage, the probability that CD62L down-regulates is approximately 0.77. In the CM stage, the probabilities that CD27 and CD127 down-regulate are 0.75 and 0.79, respectively. In the beginning of the EM stage, the probability of CD57 up-regulating is approximately 0.77. These checkpoints have the potential of creating a diversity of phenotypes involving CD62L, CD27, CD127, and CD57.

## 4. Discussion

Flow cytometry is recognized as a valuable tool for dissecting cellular populations and for deciphering complex cellular processes at the single-cell level. However, as the number of measurable cellular parameters increases, the analysis methods become limiting, time consuming, and not easily reproducible. In this study, to better characterize high-dimensional cytometric data, we demonstrated that PSM can reproducibly and objectively model cytometric data, and that multiple files can be combined to generate an averaged model. We also determined that phenotypic patterns of surface protein expression are similar between donors and that changes in specific protein expression are correlated with other proteins. By generating a progression of CD8<sup>+</sup> T cells based on actual data, we determined four major memory and effector subsets (Fig. 4A). Additionally, branching markers were identified, revealing minor subpopulations in the effector/memory subsets (Fig. 6).

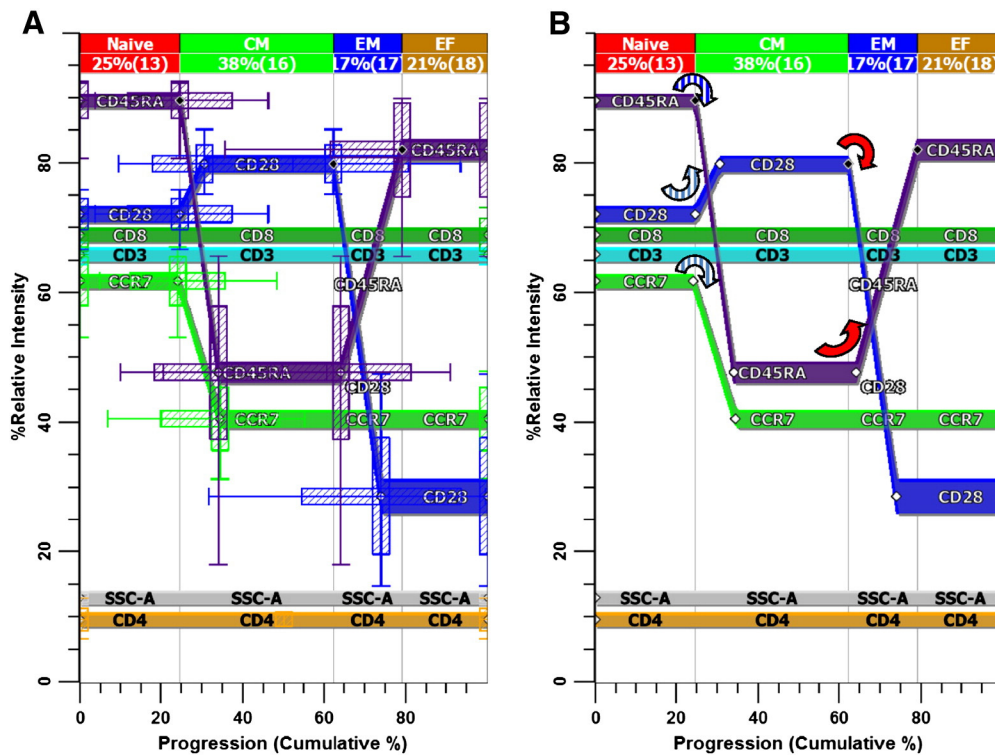


**Fig. 4.** Average probability state model for CD8<sup>+</sup> T-cell Ag-dependent progression. Panel A shows an average probability state model progression plot derived from 20 PBMC samples from healthy donors. The means and SDs (in parentheses) of the stage percentages are shown at the top. The vertical box whiskers show that there was quite a bit of variability in the measurement intensities. This variability is presumably a function of not only donor-to-donor variability, but also instrument setup variability. The horizontal box whiskers show the variations of the CD8<sup>+</sup> subset percentages. Panel B shows some important CDP cumulative percentage correlations. When CD45RA is down-regulated, CCR7 is also down-regulated (blue hatched arrows,  $r = 0.85$ ,  $p < 0.00001$ ). The average difference between these two locations (diff =  $-0.51\%$ ) was found to be not statistically significant using a paired  $t$  test. These data are not consistent with the existence of an extra stage as defined by CD45RA-CCR7 (CD197)<sup>+</sup>CD28<sup>+</sup> for CD8<sup>+</sup> cells. Also, at the point where CD45RA down-regulates, CD28 slightly up-regulates (see blue hatched arrow). When CD28 then down-regulates, CD45RA begins to up-regulate (red solid arrows,  $r = 0.56$ ,  $p < 0.01$ , diff = 1.9, NS).

GemStone™ uses a mathematical modeling system to divide progressions into individual states and searches for a solution that makes these states equally probable for event selection. For each measurement, or marker, a progression probability-based variable is generated. Since all the measurements relate to this same progression variable, a single graphical progression plot shows all the measurement correlations in high-dimensional data. The PSM approach can be applied to many types of data and is a useful method for revealing biological mechanisms and validating models of subset differentiation underlying cellular ontogeny.

Another important element of PSM is the approach to modeling data. The strategy is to begin by defining the simplest EPs that are well characterized (e.g., CCR7) and work toward the more complex EPs that are less characterized. Similar to the need for biological knowledge necessary for the interpretation of traditional gating analysis, the use of a biological reference point gives context to analysis of the modeled data. In the model, the events are distributed equally across the states for each EP, whether it is considered alone or in concert with other markers. Therefore, the analysis can be approached one measurement at a time, allowing for a scalable analysis method to a high-dimensional set of measurements, including unknown elements. Additionally, in traditional gating, overlaps in populations require subjective gating decisions. Flow cytometry standardization studies have identified gating as the largest

component in variability of results between laboratories (Jaimes et al., 2011; Maecker et al., 2005). In PSM, regions defined along a progression axis can automatically account for population overlaps.

Many studies have demonstrated the link between phenotypic expression markers on CD8<sup>+</sup> T cells with functional properties, including ex vivo effector function. (Appay et al., 2008; Hamann et al., 1997; Lefrancois and Obar, 2010; Sallusto et al., 1999). With these observations, much research has focused on the classification of effector and memory T-cell subpopulations and their respective functions. The phenotypic heterogeneity in memory T-cell populations has confounded the definition of an accepted model describing immunological development of CD8<sup>+</sup> T cells. To approach the classification of memory/effector subpopulations from a new angle, PSM was applied to healthy donors' PBMCs stained with CD8<sup>+</sup> T-cell markers. The progression plots show three major transitions forming four stages based on CD45RA and CD28, where changes in marker intensities presumably reflect the changes in functional states. This analysis of CD8<sup>+</sup> T-cell differentiation is somewhat in contrast to a previous publications outlining five subsets of effector and memory cells (Appay et al., 2008). By averaging the files of multiple healthy donors, the correlation of transitions in percent relative intensity of markers could be determined. The averaged modeled data of 20 healthy donors showed that down-regulation of CD45RA and CCR7 at

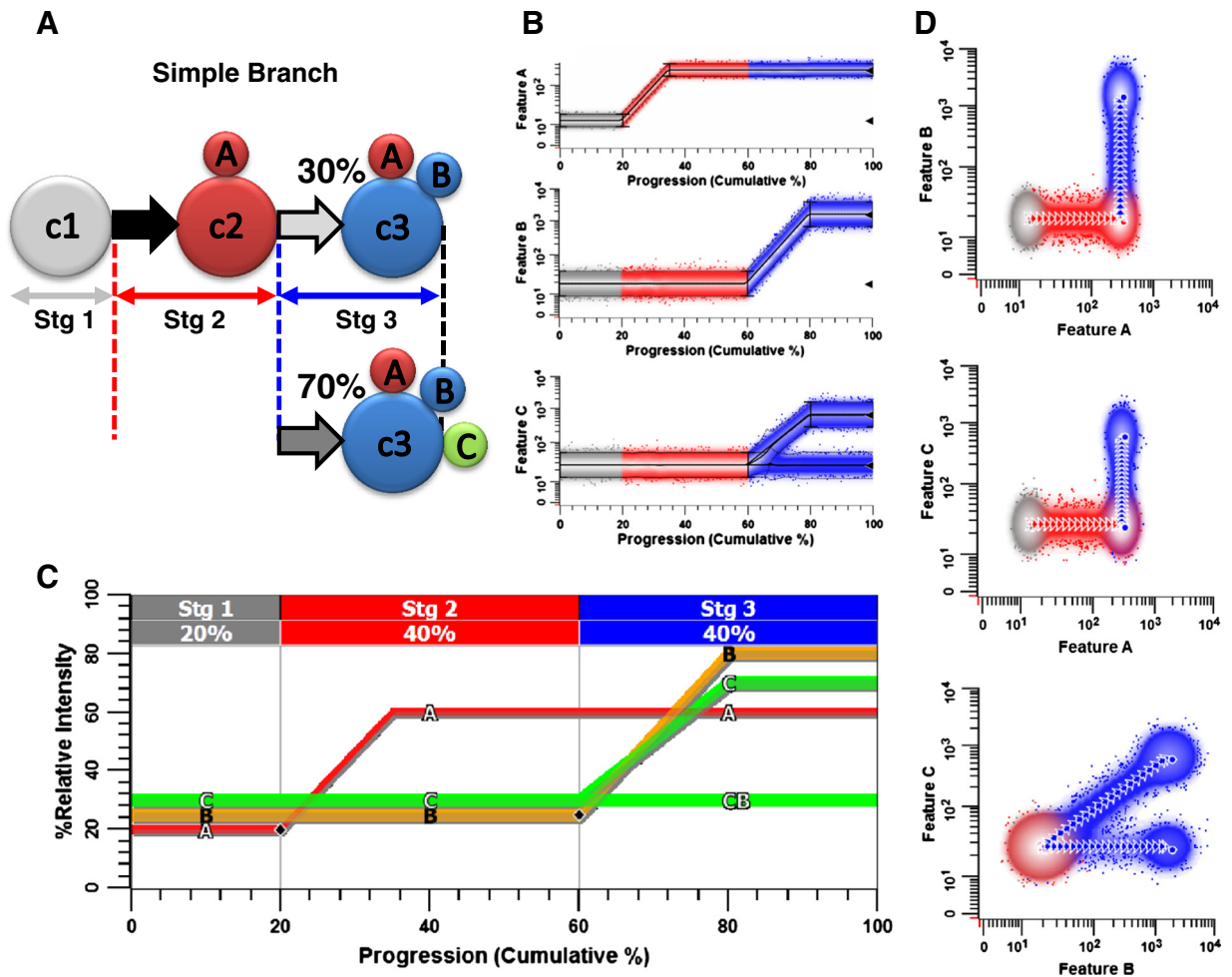


**Fig. 5.** Branched EPs. Panel A shows a progression schematic similar to Fig. 1 but includes a simple branch involving feature C. In this example, when cells reach the feature B up-regulation checkpoint, 70% of the cells also up-regulate feature C while 30% do not. Panel B delineates the three probability state model EPs that model this simple branch (top = feature A, middle = feature B, and bottom = feature C). Panel C summarizes this progression in the probability state model progression plot that includes the branching of feature C (see CB label). Panel D shows the PSM surface dot plots for feature A vs. B (top), feature A vs. C (middle), and feature B vs. C (bottom). Note that branches are not always visible in dot plots, which is why they have traditionally been difficult to detect. Branches are relatively easy to determine with PSM, since non-branched EPs are incompatible with branched data, resulting in a dramatic loss of classified events and poor fitting. In this simple example, the branch point is at the end of Stage 2. However, when modeling T-cell branches, the location may be anywhere along the progression axis.

the end of the naïve stage is significantly correlated (Fig. 4). These transitions in expression levels define the end of the naïve stage and the beginning of the CM stage. There is no evidence that later changes in CCR7 form an additional stage. The indicator for the end of the CM stage and the beginning of the EM stage is defined by the down-regulation of CD28 and the up-regulation of CD45RA. The modeled data set described in this analysis suggests that it might be inappropriate to add an extra early CD8<sup>+</sup> T-cell stage defined by the phenotype CD45RA<sup>-</sup>CCR7<sup>+</sup>CD28<sup>+</sup>, as previously published (Appay et al., 2008).

Additionally, modeling reduces the data complexity into a relatively small set of model parameters. These model parameters are amenable to group statistics and comparisons. These features could play an important role in the better understanding of normal and pathologic changes in cellular immunity. For example, they can be applied to better understand how the distribution of subsets of memory T cells

can change with age (Koch et al., 2008), to analyze seasonal variations (Khoo et al., 2012; van Rood et al., 1991), or to determine the variability of cellular immunity in the healthy donor (Maecker et al., 2012).

In PSM, the differential expression of a marker along a developmental pathway is graphically visualized as branching (see Fig. 6). Therefore, the heterogeneous expression of a marker in PSM is viewed as a branch in an EP. Branches are relatively easy to detect with PSM, since non-branched EPs are incompatible with branched data, resulting in a dramatic loss of classified events and poor fitting. By PSM analysis, CD62L, CD57, CD27, and CD127 all were identified and characterized as branching markers. Each of these markers is commonly used in the identification of CD8<sup>+</sup> T-cell CM and EM populations (Bannard et al., 2009; Stemmerger et al., 2007; Wiesel et al., 2009). CD62L (L-selectin) has been described as being cleaved from the cell membrane following antigen activation (Yang

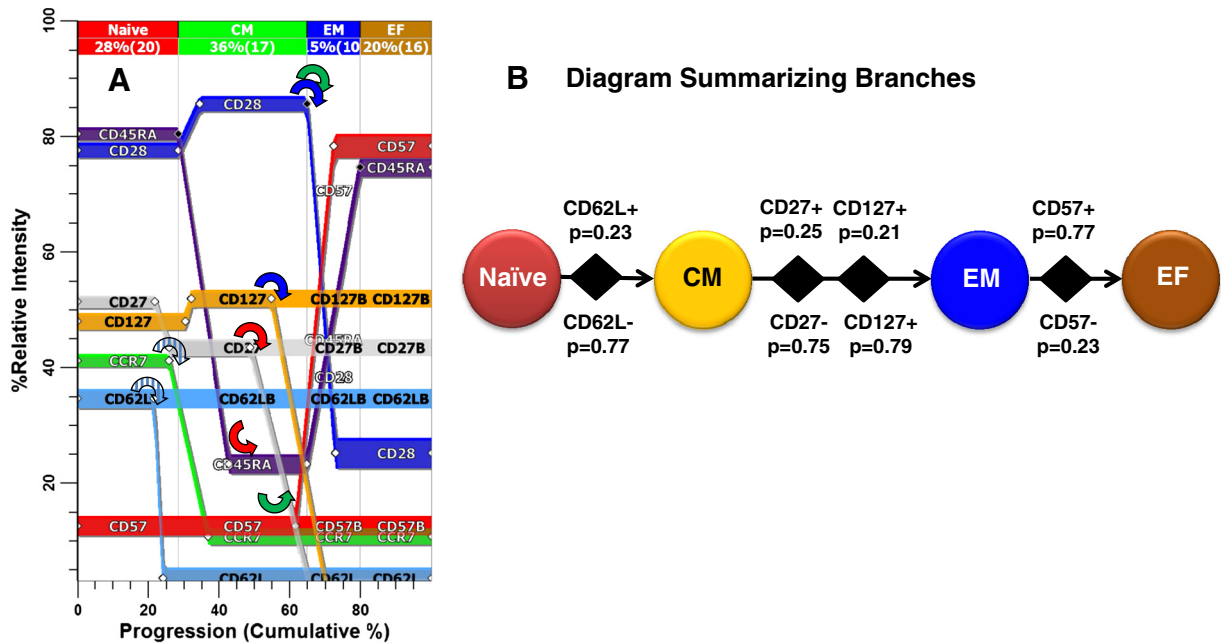


**Fig. 6.** Average CD8<sup>+</sup> T-cell branched EPs. As shown in Panel A, CD62L (L-selectin) has a 77% (9%) chance of down-regulating slightly before the end of the naïve stage and correlates best with the down-regulation of CCR7 (blue hatched arrows  $r = 0.81, p < 0.00001, \text{diff} = -4.23, \text{NS}$ ). CD27 slightly down-regulates with CD45RA and CCR7 at the end of the naïve stage and then has a 75% (17%) chance of fully down-regulating in the middle of the CM stage. Interestingly, CD27 is best correlated with the beginning of the second level of expression for CD45RA (solid red arrows,  $r = 0.90, p < 0.00001, \text{diff} = 6.00, p < 0.0008$ ). CD127 slightly up-regulates at the end of the naïve stage and then has a 79% (16%) chance of fully down-regulating in the middle of the CM stage. It is highly correlated with the down-regulation of CD28 (solid blue arrows,  $r = 0.86, p < 0.00001, \text{diff} = -6.79, p < 0.02$ ). CD57 has a 77% (15%) chance of up-regulating at the end of the CM stage. It is also best correlated with the down-regulation of CD28 (solid green arrows,  $r = 0.97, p < 0.00001, \text{diff} = -3.23, \text{NS}$ ). Panel B summarizes the branch data in terms of a series of probabilistic checkpoints. In the naïve stage, the probability that CD62L down-regulates is approximately 0.77. In the CM stage, the probabilities that CD27 and CD127 down-regulate are 0.75 and 0.79, respectively. In the beginning of the EM stage, the probability of CD57 up-regulating is approximately 0.77.

et al., 2011). It is also well known that CD62L expression can change dramatically during standard experimental procedures (Stibenz and Buhner, 1994). These observations indicate that CD62L is not useful as a selective marker for the identification of CM and EM subsets and are further supported by the branching profile observed with GemStone™ analysis. CD127 and CD27 are also often used in the classification of memory subsets by dot-plot analysis (Stemberger et al., 2007; Tomiyama et al., 2002, 2004). The branching of CD127 and CD27 expression in CD8<sup>+</sup> T-cell CM and EM populations, which is not easily identified in standard dot plot analysis, may result in misidentification of CD8 memory subsets.

In a progression plot, it is evident that the markers discussed previously branch into different subsets at different stages and are not specific for the memory subsets. These branches are not easily visualized in traditional dot plots. Gated populations based on these markers can result in the grouping of multiple populations, leading to conclusions which may be misleading. The use of the branched markers in identification of memory subsets could be one explanation for the lack of consensus in the identification of T-cell memory populations. A probability state model progression plot is one approach to visualizing the phenotypic heterogeneity of the multiple fates in T-cell development. The findings reported in this study concur with a recent study which suggests that there is asymmetric cell division in re-challenged

memory T cells, resulting in phenotypically distinct populations of daughter cells (Ciocca et al., 2012).

In summary, using PSM, GemStone™ allows for a unique visualization resulting in multiple phenotypic biomarker correlations without the limitations of bivariate dot plots or subjective gating. This results in the ability to examine the relative timing of phenotypic changes during CD8 T-cell differentiation. Using three markers, CD45RA, CD28, and CCR7, we identified four major CD8<sup>+</sup> T-cell subsets in PBMCs of healthy donors. CD57, CD62L, CD27, and CD127 are frequently used in the identification of T-cell memory subsets but in this study were identified as branching markers. The branching aspect is difficult to identify in traditional methods of data analysis and may account for inconsistencies in the definition of immunological memory. Branched markers such as CD57, CD62L, CD27, and CD127 should not be used as primary staging markers. However, these markers may be useful in identification of the heterogeneous phenotypes in T-cell memory populations. Thus, subjective gating may be replaced as more objective and automated methods like PSM become more available.

**Acknowledgments**

We thank Beth Hill and Smita Ghanekar for reviewing the manuscript and Perry Haaland and Bob Zigon for their helpful comments on the manuscript.

## Competing Financial Interests

C.B.B. is a named inventor on patent applications claiming the use of the technology described in this publication and is the owner of Verity Software House, a company which sells the software used in the work reported here. V.C.M and M.S.I. are paid employees of BD Biosciences, a company which developed the flow cytometers and reagents used in this work.

## Appendix A. Supplementary data

Supplementary data to this article can be found online at <http://dx.doi.org/10.1016/j.jim.2013.08.003>.

## References

- Aghaepour, N., Chattopadhyay, P.K., Ganesan, A., O'Neill, K., Zare, H., Jalali, A., Hoos, H.H., Roederer, M., Brinkman, R.R., 2012. Early immunologic correlates of HIV protection can be identified from computational analysis of complex multivariate T-cell flow cytometry assays. *Bioinformatics* 28, 1009.
- Appay, V., Dunbar, P.R., Callan, M., Klenerman, P., Gillespie, G.M., Papagno, L., Ogg, G.S., King, A., Lechner, F., Spina, C.A., Little, S., Havlir, D.V., Richman, D.D., Gruener, N., Pape, G., Waters, A., Easterbrook, P., Salio, M., Cerundolo, V., McMichael, A.J., Rowland-Jones, S.L., 2002. Memory CD8<sup>+</sup> T cells vary in differentiation phenotype in different persistent virus infections. *Nat. Med.* 8, 379.
- Appay, V., van Lier, R.A., Sallusto, F., Roederer, M., 2008. Phenotype and function of human T lymphocyte subsets: consensus and issues. *Cytometry A* 73, 975.
- Arens, R., Schoenberger, S.P., 2010. Plasticity in programming of effector and memory CD8 T-cell formation. *Immunol. Rev.* 235, 190.
- Bachmann, M.F., Wolint, P., Schwarz, K., Jager, P., Oxenius, A., 2005. Functional properties and lineage relationship of CD8<sup>+</sup> T cell subsets identified by expression of IL-7 receptor alpha and CD62L. *J. Immunol.* 175, 4686.
- Bagwell, C.B., 2007. In: USPTO (Ed.), *Probability state models*, vol. 7, 653, 509. Verity Software House, USA.
- Bagwell, C.B., 2010. Probability state modeling: a new paradigm for cytometric analysis. In: Litwin, V., Marder, P. (Eds.), *Flow Cytometry in Drug Discovery and Development*. John Wiley & Sons, Inc., Hoboken, NJ, p. 281.
- Bagwell, C.B., 2011. Breaking the Dimensionality Barrier. In: Hawley, T.S., Hawley, R.G. (Eds.), *Flow Cytometry Protocols*. Humana Press, New York City, p. 31.
- Bagwell, C.B., 2012. A New Paradigm for Cytometric Analysis. In: Kottke-Marchant, K., Davis, B.H. (Eds.), *Laboratory Hematology Practice*. Wiley-Blackwell Publishing Ltd.
- Bannard, O., Kraman, M., Fearon, D., 2009. Pathways of memory CD8<sup>+</sup> T-cell development. *Eur. J. Immunol.* 39, 2083.
- Bashashati, A., Brinkman, R.R., 2009. A survey of flow cytometry data analysis methods. *Adv. Bioinforma.* 584603.
- Chattopadhyay, P.K., Price, D.A., Harper, T.F., Betts, M.R., Yu, J., Gostick, E., Peretto, S.P., Goepfert, P., Koup, R.A., De Rosa, S.C., Bruchez, M.P., Roederer, M., 2006. Quantum dot semiconductor nanocrystals for immunophenotyping by polychromatic flow cytometry. *Nat. Med.* 12, 972.
- Ciocca, M.L., Barnett, B.E., Burkhardt, J.K., Chang, J.T., Reiner, S.L., 2012. Cutting edge: asymmetric memory t cell division in response to rechallenge. *J. Immunol.* 188, 4145.
- Costa, E.S., Pedreira, C.E., Barrera, S., Lecrevisse, Q., Flores, J., Quijano, S., Almeida, J., del Carmen Garcia-Macias, M., Bottcher, S., Van Dongen, J.J., Orfao, A., 2010. Automated pattern-guided principal component analysis vs expert-based immunophenotypic classification of B-cell chronic lymphoproliferative disorders: a step forward in the standardization of clinical immunophenotyping. *Leukemia* 24, 1927.
- Geginat, J., Lanzavecchia, A., Sallusto, F., 2003. Proliferation and differentiation potential of human CD8<sup>+</sup> memory T-cell subsets in response to antigen or homeostatic cytokines. *Blood* 101, 4260.
- Hamann, D., Baars, P.A., Rep, M.H., Hooibrink, B., Kerkhof-Garde, S.R., Klein, M.R., van Lier, R.A., 1997. Phenotypic and functional separation of memory and effector human CD8<sup>+</sup> T cells. *J. Exp. Med.* 186, 1407.
- Inokuma, M., Trotter, J., Maino, V.C., Ghanekar, S., Bagwell, C.B., 2010. A novel modeling system for analysis of high dimensional data: Definition of T cell effector and memory subsets using GemStone software. XXV Congress of the International Society for Advancement of Cytometry, Seattle, Washington.
- Jaimes, M.C., Maecker, H.T., Yan, M., Maino, V.C., Hanley, M.B., Greer, A., Darden, J.M., D'Souza, M.P., 2011. Quality assurance of intracellular cytokine staining assays: analysis of multiple rounds of proficiency testing. *J. Immunol. Methods* 363, 143.
- Kaech, S.M., Tan, J.T., Wherry, E.J., Konieczny, B.T., Surh, C.D., Ahmed, R., 2003. Selective expression of the interleukin 7 receptor identifies effector CD8 T cells that give rise to long-lived memory cells. *Nat. Immunol.* 4, 1191.
- Khoo, A.L., Koenen, H.J., Chai, L.Y., Sweep, F.C., Netea, M.G., van der Ven, A.J., Joosten, I., 2012. Seasonal variation in vitamin D(3) levels is paralleled by changes in the peripheral blood human T cell compartment. *PLoS One* 7, e29250.
- Koch, S., Larbi, A., Derhovanessian, E., Oczelik, D., Naumova, E., Pawelec, G., 2008. Multiparameter flow cytometric analysis of CD4 and CD8 T cell subsets in young and old people. *Immun. Ageing* 5, 6.
- Lefrancois, L., Obar, J.J., 2010. Once a killer, always a killer: from cytotoxic T cell to memory cell. *Immunol. Rev.* 235, 206.
- Loken, M.R., Wells, D.A., 2000. Normal antigen expression in hematopoiesis: basis for interpreting leukemia phenotypes. In: Stewart, C.C., Nicholson, J.K.A. (Eds.), *Immunophenotyping*. Wiley-Liss, New York, NY, p. 133.
- Lugli, E., Roederer, M., Cossarizza, A., 2010. Data analysis in flow cytometry: the future just started. *Cytometry A* 77, 705.
- Maecker, H.T., Rinfret, A., D'Souza, P., Darden, J., Roig, E., Landry, C., Hayes, P., Birungi, J., Anzala, O., Garcia, M., Harari, A., Frank, I., Baydo, R., Baker, M., Holbrook, J., Ottinger, J., Lamoreaux, L., Epling, C.L., Sinclair, E., Suni, M.A., Punt, K., Calarota, S., El-Bahi, S., Alter, G., Maila, H., Kuta, E., Cox, J., Gray, C., Altfeld, M., Nougarede, N., Boyer, J., Tussey, L., Tobery, T., Bredt, B., Roederer, M., Koup, R., Maino, V.C., Weinhold, K., Pantaleo, G., Gilmour, J., Horton, H., Sekaly, R.P., 2005. Standardization of cytokine flow cytometry assays. *BMC Immunol.* 6, 13.
- Maecker, H.T., McCoy, J.P., Nussenblatt, R., 2012. Standardizing immunophenotyping for the Human Immunology Project. *Nat. Rev. Immunol.* 12, 191.
- Obar, J.J., Lefrancois, L., 2010. Memory CD8<sup>+</sup> T cell differentiation. *Ann. N. Y. Acad. Sci.* 1183, 251.
- Qiu, P., Simonds, E.F., Bendall, S.C., Gibbs Jr., K.D., Bruggner, R.V., Linderman, M.D., Sachs, K., Nolan, G.P., Plevritis, S.K., 2011. Extracting a cellular hierarchy from high-dimensional cytometry data with SPADE. *Nat. Biotechnol.* 29, 886.
- Sachs, K., Gentles, A.J., Youland, R., Itani, S., Irish, J., Nolan, G.P., Plevritis, S.K., 2009. Characterization of patient specific signaling via augmentation of Bayesian networks with disease and patient state nodes. Conference proceedings: ... Annual International Conference of the IEEE Engineering in Medicine and Biology Society. IEEE Engineering in Medicine and Biology Society, Conference 2009, p. 6624.
- Sallusto, F., Lenig, D., Forster, R., Lipp, M., Lanzavecchia, A., 1999. Two subsets of memory T lymphocytes with distinct homing potentials and effector functions. *Nature* 401, 708.
- Stemberger, C., Neuenhahn, M., Buchholz, V.R., Busch, D.H., 2007. Origin of CD8<sup>+</sup> effector and memory T cell subsets. *Cell. Mol. Immunol.* 4, 399.
- Stemberger, C., Neuenhahn, M., Gebhardt, F.E., Schiemann, M., Buchholz, V.R., Busch, D.H., 2009. Stem cell-like plasticity of naive and distinct memory CD8<sup>+</sup> T cell subsets. *Semin. Immunol.* 21, 62.
- Stibenz, D., Buhner, C., 1994. Down-regulation of L-selectin surface expression by various leukocyte isolation procedures. *Scand. J. Immunol.* 39, 59.
- Tomiyama, H., Matsuda, T., Takiguchi, M., 2002. Differentiation of human CD8<sup>+</sup> T cells from a memory to memory/effector phenotype. *J. Immunol.* 168, 5538.
- Tomiyama, H., Takata, H., Matsuda, T., Takiguchi, M., 2004. Phenotypic classification of human CD8<sup>+</sup> T cells reflecting their function: inverse correlation between quantitative expression of CD27 and cytotoxic effector function. *Eur. J. Immunol.* 34, 999.
- van Rood, Y., Goulmy, E., Blokland, E., Pool, J., van Rood, J., van Houwelingen, H., 1991. Month-related variability in immunological test results; implications for immunological follow-up studies. *Clin. Exp. Immunol.* 86, 349.
- Wiesel, M., Walton, S., Richter, K., Oxenius, A., 2009. Virus-specific CD8 T cells: activation, differentiation and memory formation. *APMIS* 117, 356.
- Yang, S., Liu, F., Wang, Q.J., Rosenberg, S.A., Morgan, R.A., 2011. The shedding of CD62L (L-selectin) regulates the acquisition of lytic activity in human tumor reactive T lymphocytes. *PLoS One* 6, e22560.
- Zare, H., Shoostari, P., Gupta, A., Brinkman, R.R., 2010. Data reduction for spectral clustering to analyze high throughput flow cytometry data. *BMC Bioinf.* 11, 403.